Quantum effects in magnetization of J_1-J_2 square lattice antiferromagnet

P. Thalmeier,[1] M. E. Zhitomirsky,[2] B. Schmidt,[1] and N. Shannon[3]
[1]*Max Planck Institute for Chemical Physics of Solids, 01187 Dresden, Germany*
[2]*Commissariat á l'Energie Atomique, DSM/INAC/SPSMS, 38054 Grenoble, France*
[3]*H. H. Wills Physics Laboratory, University of Bristol, Bristol BS8 1TL, United Kingdom*
(Received 26 November 2007; published 28 March 2008)

The J_1-J_2 square lattice Heisenberg model with spin $S=1/2$ has exchange bonds both along sides (J_1) and along diagonals (J_2) of the square. It exhibits three phases with long-range magnetic order and two unconventionally ordered phases depending on the ratio J_2/J_1 of exchange constants. It describes a number of recently found layered vanadium oxide compounds. A simple means of investigating the ground state is the study of the magnetization curve and high field susceptibility. We discuss these quantities by using the second-order spin-wave theory and the exact diagonalization in the whole J_1-J_2 plane. We compare both results and find good overall agreement in the sectors of the phase diagram with magnetic order. Close to the disordered regions, the magnetization curve shows strong deviations from the classical linear behavior caused by large quantum fluctuations, and the spin-wave approximation breaks down. On the ferromagnet side ($J_1<0$), where one approaches the quantum gapless spin nematic ground state, this region is surprisingly large. This result is of great interest for the vanadium oxide compounds, which are found to lie in this region. We also investigate the effect of the interlayer coupling and find that the quasi-two-dimensional picture remains valid up to $|J_\perp/J_1| \sim 0.3$.

DOI: 10.1103/PhysRevB.77.104441 PACS number(s): 75.10.Jm, 75.30.Ds, 75.60.Ej

I. INTRODUCTION

The search for a quantum spin liquid—an insulating magnet with a gapless ground state which breaks neither lattice nor spin symmetries—has focused largely on spin-1/2 two-dimensional quantum antiferromagnets (2DQAFs). In practice, however, most two-dimensional antiferromagnet (AF) spin-1/2 Heisenberg models exhibit either Néel order or crystals of short-ranged singlet bonds and a finite gap to spin excitations.[1] In a few cases, gapless *hidden order* states with nematic character arise,[2] but among "realistic" models, possibly only the $S=1/2$ Heisenberg model on a Kagomé lattice remains a serious candidate for a spin-liquid description (see, e.g., Ref. 3 and references therein).

Perhaps the best studied example of a 2DQAF is the spin-1/2 J_1-J_2 Heisenberg model, which demonstrates a quantum phase transition from Néel to valence bond solid as a function of the control parameter J_2/J_1.[1] A number of layered vanadium compounds recently synthesized are well described by this model. They are of the type Li_2VOXO_4 ($X=Si,Ge$)[4–6] and $AA'VO(PO_4)_2$ ($A,A'=Pb,Zn,Sr,Ba$),[7–9] consisting of vanadium oxide pyramid layers containing V^{4+} ions with spin $S=1/2$.

In Refs. 10 and 11, an extensive analysis of the J_1-J_2 model, also for a finite magnetic field, has been given in order to understand the physical properties of the above compounds. Both the numerically exact diagonalization (ED) Lanczos method for finite clusters and the analytical spin-wave analysis have been employed. The behavior of the saturation field as a function of the frustration angle has been studied as a further means of diagnosis of J_1-J_2 compounds. It was found that close to the disordered regime with $J_1<0$, the behavior of the saturation field is determined by an instability of two spin excitations, indicating indeed that, in this regime, the ground state may be of a spin-nematic type.[12] This leads us to expect that the magnetization itself should also be anomalous in this regime, with a large effect from quantum fluctuations. So far, quantum corrections to the magnetization curve in the spin-wave theory have only been considered for the nonfrustrated square lattice antiferromagnet ($J_2=0$).[13]

In this work, we give a systematic investigation of the magnetization and the high field susceptibility for the general two-dimensional (2D) square lattice J_1-J_2 model. Our goal is to investigate how the quantum corrections on these quantities depend on the degree of frustration, especially close to the disordered phases. Our main interest is to establish a clear connection between the nonclassical anomalies in the magnetization and the frustration control parameter J_2/J_1. This should be useful information for further investigations of the vanadium compounds introduced above. The effect of interplane coupling will be also considered.

The low scale of exchange interactions, which are of order 10 K in the Li_2VOXO_4 and $AA'VO(PO_4)_2$ vanadates, means that magnetization measurements are relatively easy to perform. It is therefore hoped that the analysis with the theory developed here gives an additional criterion to determine the frustration ratio J_2/J_1 in a specific compound. In Sec. II, we briefly introduce the model. Its high field properties such as magnetization and susceptibility are investigated in Sec. III. They are obtained from ED Lanczos calculations as well as from first- and second-order spin-wave theories, and a comparison is given. We also evaluate the contributions of interlayer coupling in Sec. IV, and finally in Sec. V, we give a discussion and conclusion.

II. J_1-J_2 MODEL AND ITS PHASES

The 2D square-lattice spin-1/2 Heisenberg model in an external magnetic field H is given by

$$\mathcal{H} = J_1 \sum_{\langle ij \rangle_1} \mathbf{S}_i \cdot \mathbf{S}_j + J_2 \sum_{\langle ij \rangle_2} \mathbf{S}_i \cdot \mathbf{S}_j - h \sum_i S_i^z, \quad (1)$$

where J_1 and J_2 are the two exchange constants between the first and second neighbors on a square lattice, respectively. As in Refs. 10 and 11, the exchange parameters are defined per exchange bond. Furthermore, we use the convention $h = g\mu_B H$ ($g\mu_B$=gyromagnetic ratio, μ_B=Bohr magneton). The phases in zero field are best characterized by introducing equivalent parameters

$$J_c = (J_1^2 + J_2^2)^{1/2}, \quad \phi = \tan^{-1}(J_2/J_1), \quad (2)$$

or $j = \tan\phi = J_2/J_1$. The angle ϕ determines the extent of magnetic frustration in the model.

Three classical magnetic ground states are possible depending on ϕ, namely, ferromagnet (FM), Néel antiferromagnet (NAF), and collinear antiferromagnet (CAF). They have been extensively discussed in Ref. 10. The effect of exchange frustration leading to enhanced quantum fluctuations is strongest at the classical phase boundaries where the CAF phase joins the NAF or FM phase (see insets of Fig. 1). In fact, in these regions they are believed to destroy long-range magnetic order and establish two additional partially ordered states, namely, a columnar-dimer state with a spin gap at CAF/NAF boundary[14–18] and a gapless spin-nematic state at the CAF/FM boundary.[12] It can already be seen within a spin-wave approximation that the magnetic order breaks down in this regime since the sublattice moment reduction due to quantum fluctuations diverges close to the two boundary regions.[10]

III. HIGH FIELD PROPERTIES OF THE J_1-J_2 MODEL

The determination of the frustration ratio J_2/J_1 or angle $\phi = \tan^{-1}(J_2/J_1)$ is of foremost importance to characterize a given square-lattice magnetic compound such as the SiO_4 and PO_4 vanadates mentioned in the Introduction. The available experimental methods to reach this objective have been extensively discussed in Ref. 10. However, the thermodynamic zero-field methods such as evaluating the heat capacity and the magnetic susceptibility are too ambiguous to be able to locate ϕ in the NAF or CAF sector of the phase diagram. Additional information may be obtained from investigating high field properties,[11] for example, from saturation fields as, e.g., determined from the magnetocaloric effect.

The analysis of the high field magnetization itself as a function of frustration angle ϕ is also promising. From the simple nearest neighbor Heisenberg AF ($J_2=0$ or $\phi=0$), it is known from analytical work[13] that deviations from the classical linear magnetization curve due to quantum fluctuations are to be expected. This is also concluded from numerical calculations.[19] A systematic study of magnetization curves for the J_1-J_2 model is, however, lacking. Since the method is of experimental importance due to its relative simplicity, we consider it worthwhile to investigate this problem in detail for the antiferromagnetic phases of the J_1-J_2 model. For this purpose, we will use both analytical spin-wave methods similar to Ref. 13 and numerical Lanczos methods for exact diagonalization of finite clusters. Our notation will be close to the one used in Ref. 11.

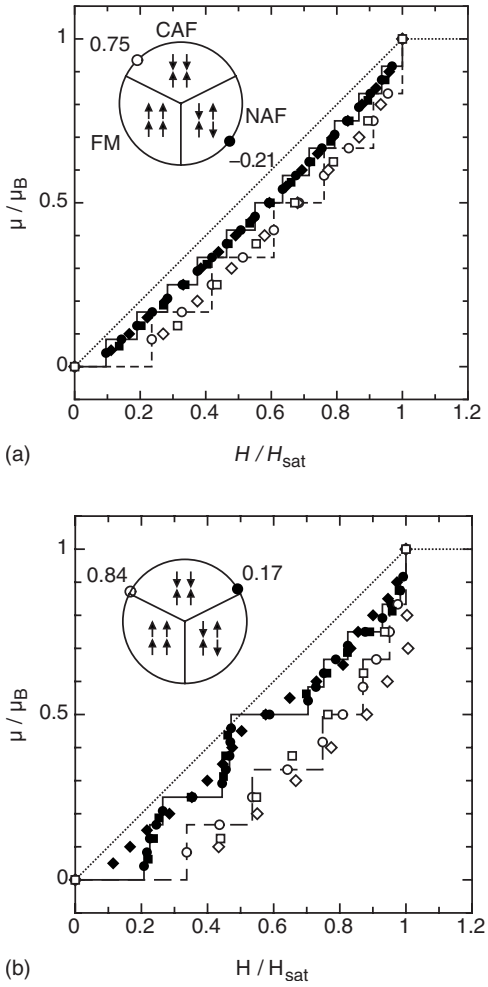

FIG. 1. The normalized magnetization obtained from the Bonner–Fisher construction as a function of an applied magnetic field H in units of the saturation field H_{sat} for different frustration angles [for $J_1>0$ $H_{sat}=h_s/(g\mu_B)$]. Data from the 24-site cluster are denoted by circles, 20-site data by diamonds, and 16-site data by squares. Additionally, the zero-temperature magnetization steps are plotted for the 24-site clusters; the solid line corresponds to the solid symbols, the dashed line to the open symbols. The insets in the plots show the positions of the frustration angles ϕ/π in the classical phase diagram. The frustration angle is counted positive above ($0<\phi/\pi<1$) and negative below ($-1<\phi/\pi<0$) the x axis in the inset diagram. For reference, the classical magnetization curve is plotted as a dotted line in both plots. (a) Classically ordered phases: Néel phase (NAF), $\phi=-0.21\pi$ (solid symbols), and collinear phase (CAF), $\phi=0.75\pi$ (open symbols). (b) Disordered regimes: Columnar-dimer phase (crossover from NAF to CAF), $\phi=0.17\pi$ (solid symbols), and spin-nematic phase (crossover from CAF to FM), $\phi=0.84\pi$ (open symbols).

A. Magnetization from numerical ($T=0$) Lanczos results for J_1-J_2 clusters

We have numerically diagonalized the Hamiltonian of the J_1-J_2 model for cluster sizes of 16, 20, and 24 sites, applying

the finite-temperature Lanczos method as described in Ref. 11 and references cited therein. In the limit $T\to 0$, our results are identical to the standard zero-temperature implementation of the algorithm, i.e., the evaluation of the partition function reduces to the determination of ground-state expectation values. The 16- and 20-site clusters are (regular and tilted) squares, and the 24-site cluster is a rectangle. All three clusters tile the infinite lattice such that, with periodic boundary conditions, compatibility with the three classically ordered ground states is preserved.

The zero-temperature field dependence of the magnetization $m=\langle S^z\rangle$ has been calculated for the whole phase diagram, except for the FM region, where the saturation field h_s vanishes. Following Ref. 20, Fig. 1 shows the normalized magnetization m/m_{sat} ($m_{\mathrm{sat}}\equiv S$) for selected values of the frustration angle ϕ in the classically ordered antiferromagnetic phases and in the two disordered regimes of the phase diagram. The magnetic field is normalized to the saturation field determined by exact diagonalization. This is identical to the classical saturation field for *positive* (antiferromagnetic) J_1. For *negative* (ferromagnetic) J_1, a $\Delta S=2$ two-magnon instability determines the saturation field for the finite-size systems considered here, which occurs at slightly higher field values than those for the one-magnon instability.[11]

The field dependence of the magnetization at $T=0$ for a finite-size system is a sequence of finite steps. The solid line in the left panel of Fig. 1 shows the magnetization curve of the 24-site cluster for $\phi=-0.21\pi$, which is in the Néel phase. The dashed line shows the same for $\phi=0.75\pi$ in the collinear phase. In the right panel, the solid line shows the field dependence for $\phi/\pi=0.17$ (columnar-dimer phase); the dashed line for $\phi/\pi=0.84$ (spin-nematic phase). The symbols in the plots denote the midpoints of the horizontal and vertical line segments of the magnetization steps: circles label the 24-site data, diamonds the 20-site data, and squares the 16-site data. (For the smaller cluster sizes, the step functions are not shown.) Note that due to the $\Delta S=2$ steps in the magnetization for $\phi>\pi/2$ (ferromagnetic J_1), there exist only one-half as many data points as those for $\phi<\pi/2$. According to Bonner and Fisher,[20] these midpoints should yield, at least for $J_2=0$, a good approximation of the magnetization curve of the square lattice Heisenberg model in the thermodynamic limit.

The angles $\phi/\pi=-0.21$ and 0.75 for the NAF and CAF in the left plot of Fig. 1 are chosen such that they correspond to the experimental findings for the compound $SrZnVO(PO_4)_2$.[10] For these values, the midpoints of the magnetization steps form a smooth function. This can generally be observed for any frustration angle located inside the magnetically ordered regimes, be it NAF or CAF. In contrast, for $\phi/\pi=0.17$ (solid symbols and line in the right plot of Fig. 1) and $\phi/\pi=0.85$ (open symbols and dashed line), the data points scatter much more and do not give rise to a smooth field dependence. Furthermore, in the columnar-dimer phase ($\phi/\pi=0.17$), the well-established half-magnetization plateau appears at $m=\frac{1}{2}m_{\mathrm{sat}}$.[21,22] The data in the right panel of Fig. 1 indicate the possibility of yet another plateau at $m=\frac{1}{4}m_{\mathrm{sat}}$, though a careful examination of finite-size effects is necessary to make a final conclusion.

In the whole phase diagram, quantum effects lead to negative corrections: the exact magnetization curve $m(h)$ always lies below the corresponding classical value, which is a consequence of the lowering of the ground-state energy of a quantum antiferromagnet compared to its classical counterpart.[13]

B. Spin-wave excitations in an external magnetic field

A standard Holstein–Primakoff approximation of Eq. (1) and a subsequent Bogoliubov transformation lead to the harmonic spin-wave Hamiltonian[11]

$$\mathcal{H}=NE_0+NE_{zp}+\sum_{\lambda\mathbf{k}}\epsilon_{\lambda\mathbf{k}}(h)\alpha^{\dagger}_{\lambda\mathbf{k}}\alpha_{\lambda\mathbf{k}}, \tag{3}$$

where $\alpha^{\dagger}_{\lambda\mathbf{k}}$ are magnon operators that obey bosonic commutation rules. The $\epsilon_{\lambda\mathbf{k}}(h)$ denote the spin-wave dispersion of branch $\lambda=\pm$ as defined in the appropriate NAF or CAF magnetic Brillouin zone (BZ). It is given by

$$\epsilon_{\pm\mathbf{k}}(h)=\sqrt{[A_{\mathbf{k}}(h)\pm C_{\mathbf{k}}(h)]^2-B_{\mathbf{k}}(h)^2}. \tag{4}$$

Here, $A_{\mathbf{k}}(h)$ is the intrasublattice and $B_{\mathbf{k}}(h)$, $C_{\mathbf{k}}(h)$ are the intersublattice couplings given below. The ground-state energy is composed of a classical part (E_0) obtained from the mean field approximation to Eq. (1) and a part due to zero point fluctuations of spins (E_{zp}). The former is given by

$$E_0=-h\langle S_{\parallel}\rangle+a_{\parallel}\langle S_{\parallel}\rangle^2-a_{\perp}\langle S_{\perp}\rangle^2, \tag{5}$$

where $\langle S_{\parallel}\rangle=S\cos\frac{\theta_c}{2}$, $\langle S_{\perp}\rangle=S\sin\frac{\theta_c}{2}$, and $\theta_c/2$ is the classical field induced canting angle of AF moments counted from the z axis, which is chosen parallel to the applied field $\mathbf{h}$ (here $\parallel\equiv z$ and $\perp\equiv x,y$). The coefficients in Eq. (5) are given by

$$a_{\parallel}=\frac{z}{2}(J_1+J_2),$$

$$a_{\perp}=\frac{z}{2}(J_1-J_2)\quad(\mathrm{NAF}),$$

$$a_{\perp}=\frac{z}{2}J_2\quad(\mathrm{CAF}), \tag{6}$$

where $z=4$ is the coordination number. The classical canting angle $\theta_c/2$ of moments is obtained by minimizing E_0, which leads to

$$\cos\frac{\theta_c}{2}=\frac{h}{h_s},\quad h_s=2S(a_{\parallel}+a_{\perp}), \tag{7}$$

where h_s is the classical saturation field. For $h\geq h_s$, the moments are fully polarized, i.e., all are ferromagnetically aligned parallel to $\mathbf{h}$. Explicitly, we have $h_s=2zSJ_1$ (NAF) and $h_s=zS(J_1+2J_2)$ (CAF).

The zero point energy due to quantum fluctuations is obtained as[11]

$$E_{zp}=\frac{1}{2N}\sum_{\lambda\mathbf{k}}[\epsilon_{\lambda\mathbf{k}}(h)-A_{\mathbf{k}}]. \tag{8}$$

For the CAF and NAF phases, it is always negative and vanishes in the FM or fully polarized ($h=h_s$) phase, where

the ground state and spin-wave states are exact eigenstates with a dispersion $\epsilon_{\lambda \mathbf{k}} \equiv A_{\mathbf{k}}$. The sublattice couplings which determine the spin-wave dispersion in the canted state were derived in Ref. 11 and are given here for completeness. Defining

$$A_{\mathbf{k}} = Sa_{\mathbf{k}},$$

$$B_{\mathbf{k}}(h) = Sb_{\mathbf{k}} \sin^2 \frac{\theta_c}{2},$$

$$C_{\mathbf{k}}(h) = Sc_{\mathbf{k}} \cos^2 \frac{\theta_c}{2}, \tag{9}$$

we have in the NAF and CAF phases corresponding to wave vectors $\mathbf{Q}=(\pi,\pi)$ and $\mathbf{Q}=(\pi,0)$, respectively:

$$a_{\mathbf{k}} = 4[J_1 - J_2(1-\bar{\gamma}_{\mathbf{k}})] \quad \text{(NAF)},$$

$$c_{\mathbf{k}} = -b_{\mathbf{k}} = 4J_1\gamma_{\mathbf{k}},$$

$$a_{\mathbf{k}} = 2[2J_2 + J_1\gamma_y] \quad \text{(CAF)},$$

$$c_{\mathbf{k}} = -b_{\mathbf{k}} = 2[J_1 + 2J_2\gamma_y]\gamma_x, \tag{10}$$

where the geometric structure factors are defined by

$$\gamma_{\mathbf{k}} = \frac{1}{2}(\cos k_x + \cos k_y),$$

$$\bar{\gamma}_{\mathbf{k}} = \cos k_x \cos k_y,$$

$$\gamma_x = \cos k_x, \quad \gamma_y = \cos k_y. \tag{11}$$

Due to the symmetry properties $A_{\mathbf{k}+\mathbf{Q}}=A_{\mathbf{k}}$, $B_{\mathbf{k}+\mathbf{Q}}=-B_{\mathbf{k}}$, and $C_{\mathbf{k}+\mathbf{Q}}=-C_{\mathbf{k}}$, we have the identity $\epsilon_{\pm}(\mathbf{k}+\mathbf{Q})=\epsilon_{\mp}(\mathbf{k})$. Then, instead of summing over two spin-wave branches in the magnetic BZ of NAF or CAF, we may restrict to one mode only, e.g., $\epsilon_{\mathbf{k}} \equiv \epsilon_{+\mathbf{k}}$, and sum over the whole paramagnetic BZ in the expression for E_{zp} and similar ones. Using this convention, the spin-wave branch index λ will be omitted in the following. Using Eqs. (4) and (9), the spin-wave energies may be written as

$$\epsilon_{\mathbf{k}}(h) = S(a_{\mathbf{k}} + c_{\mathbf{k}})^{1/2}(a_{\mathbf{k}} + c_{\mathbf{k}} \cos\ \theta_c)^{1/2}, \tag{12}$$

for both NAF and CAF cases with $a_{\mathbf{k}}$ and $c_{\mathbf{k}}$ given in Eq. (10).

C. Magnetization from first-order spin-wave quantum corrections

The zero-temperature magnetization is given by the field derivative of the total ground-state energy

$$m = m_0 + m_{zp} = -\frac{\partial E_0(h)}{\partial h} - \frac{\partial E_{zp}(h)}{\partial h},$$

$$m = S\frac{h}{h_s} - \frac{1}{2N}\sum_{\mathbf{k}} \frac{\partial \epsilon_{\mathbf{k}}(h)}{\partial h}, \tag{13}$$

where the first term is the linear classical part and the second one the (negative) correction due to quantum fluctuations included up to first order in $1/S$. We can write

$$\frac{\partial \epsilon_{\mathbf{k}}(h)}{\partial h} = \frac{1}{\epsilon_{\mathbf{k}}(h)}\frac{2C_{\mathbf{k}}}{h}[(A_{\mathbf{k}} + C_{\mathbf{k}}) - B_{\mathbf{k}}]$$

$$= \frac{2S}{h_s}c_{\mathbf{k}}\left(\frac{a_{\mathbf{k}} + c_{\mathbf{k}}}{a_{\mathbf{k}} + c_{\mathbf{k}} \cos\ \theta_c}\right)^{1/2} \cos\frac{\theta_c}{2}. \tag{14}$$

This finally leads to a total magnetization, including the first-order quantum corrections as follows:

$$m = S\frac{h}{h_s}\left[1 - \frac{1}{h_s}\frac{1}{N}\sum_{\mathbf{k}} c_{\mathbf{k}}\left(\frac{a_{\mathbf{k}} + c_{\mathbf{k}}}{a_{\mathbf{k}} + c_{\mathbf{k}} \cos\ \theta_c}\right)^{1/2}\right], \tag{15}$$

where on the right-hand side the classical value of θ_c given by $\cos(\theta_c/2)=h/h_s$ has to be used. Because $h_s=2S(a_{\parallel}+a_{\perp})$, the second term in Eq. (15) is formally a $1/S$ correction to the linear classical term $m_0=S(h/h_s)$.

Explicitly, using Eqs. (10) and (11), we have for the NAF case a magnetization depending on field strength and frustration angle according to

$$\text{NAF:}\ \ m = S\frac{h}{h_s}\left[1 - \frac{1}{2SN} \times \sum_{\mathbf{k}} \gamma_{\mathbf{k}}\left(\frac{1 + \gamma_{\mathbf{k}} - j(1-\bar{\gamma}_{\mathbf{k}})}{1 + \gamma_{\mathbf{k}} \cos\ \theta_c - j(1-\bar{\gamma}_{\mathbf{k}})}\right)^{1/2}\right], \tag{16}$$

where we used $j=\tan\phi=J_2/J_1$. In this expression, the $(1/S)$ character of the quantum correction becomes manifest. For the simple NAF with $j=0$, we reproduce the result first given in Ref. 13.

A similar but more complicated expression may be given for the CAF phase. Defining $\delta_{\mathbf{k}}=(1/2)(\cos k_x - \cos k_y)$ in addition to Eq. (11), we obtain

$$\text{CAF:}\ \ m = S\frac{h}{h_s}\left[1 - \frac{1}{2SN\left(j+\frac{1}{2}\right)}\sum_{\mathbf{k}}\left[\frac{1}{2}(\gamma_{\mathbf{k}} + \delta_{\mathbf{k}}) + j\bar{\gamma}_{\mathbf{k}}\right] \times \left(\frac{j(1+\bar{\gamma}_{\mathbf{k}}) + \gamma_{\mathbf{k}}}{j(1+\bar{\gamma}_{\mathbf{k}} \cos\ \theta_c) + \gamma_{\mathbf{k}} \cos^2\frac{\theta_c}{2} - \delta_{\mathbf{k}} \sin^2\frac{\theta_c}{2}}\right)^{1/2}\right]. \tag{17}$$

Note that the special CAF case with $J_1=0$ $(j=\infty)$ is equivalent to the simple NAF case $J_2=0$ $(j=0)$ in Eq. (16). This may be seen by applying a $\mathbf{k}$-coordinate rotation by $\pi/4$ in Eq. (17).

Naturally, the above expressions should be primarily valid deep inside the NAF and CAF regions where the staggered moments are large. Close to the boundaries, quantum fluctuations grow and destroy the magnetic order. Then corrections to $m(h)$ starting from the ordered state and expanded in orders of $1/S$ are no longer appropriate.

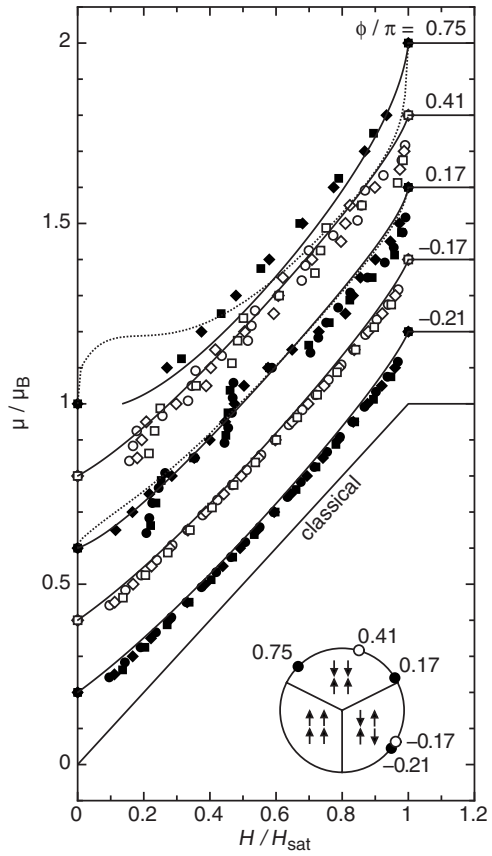

FIG. 2. Magnetization curves $\mu/\mu_B = gm$ $(=m/S)$ for various frustration angles in the antiferromagnetic or disordered sectors with an offset of 0.2 applied. Symbols are obtained from Lanczos magnetization data for $N=16$ (squares), $N=20$ (diamonds), and $N=24$ (dots, circles) size clusters using the Bonner–Fisher construction (Ref. 20). Lines are obtained from first (full) or second (dotted) order spin-wave calculations of Secs. III C and III F. Angles $\phi/\pi = 0.75, -0.21$ correspond to the possible CAF or NAF values of the Sr compound. Magnetization curves strongly differ in the extent of nonlinear deviation from the classical curve, which corresponds to $\phi/\pi = -0.5$. Furthermore, $\phi/\pi = 0.41, -0.17$ are values which are deeply within the CAF or NAF regions, and overall agreement of spin-wave and Lanczos calculations is good. It is less so on the CAF side, where the magnetization changes in steps of $\Delta S_z = 2$, leading to a larger finite-size scattering. The values $\phi/\pi = 0.75, 0.17$ correspond to regions close to or within the nonmagnetic sectors. Close to the CAF/FM boundary, the first-order spin-wave results overemphasize the nonlinear behavior and become unstable at very low fields. Close to the CAF/NAF boundary, the numerical data exhibit a plateau at $m/S = \mu/\mu_B = 0.5$, which would require a separate analysis. The plateau was first reported in Ref. 21. The inset shows the position of plotted ϕ values in the phase diagram. Second-order spin-wave results are discussed in Sec. III F.

The combined analytical spin-wave and numerical Lanczos results for the magnetization are shown in Fig. 2. One may indeed see that the agreement of both is good deep inside the NAF $(\phi/\pi = -0.21, -0.17)$ and CAF $(\phi/\pi = 0.41)$ sectors. On the other hand, close to the classical phase boundaries $(\phi/\pi = 0.17, 0.75)$, discrepancies appear. For the former case, our and previous[22] Lanczos results indicate the appearance of the one-half magnetization plateau, with $m = \frac{1}{2} m_{\mathrm{sat}}$ close to $h/h_s = 0.5$. It may be seen as a consequence of a four-spin bound state with $S_z^{\mathrm{tot}} = 1/2$ on a square plaquette which is stable for a finite range of fields.[22] (Such a plateau has also been found in the equivalent classical model at finite temperatures.[21]) For the latter, the magnetization curve becomes very nonlinear due to quantum fluctuations and $m(h)$ becomes negative at low fields (upper full line), indicating the breakdown of the $1/S$ expansion. This means that the CAF state becomes unstable and a new (spin nematic) order parameter will be realized in a finite sector around $\phi/\pi = 0.85$ $(J_2/J_1 \sim -0.5)$. Generally, one may say that quantum corrections leading to nonlinear magnetization will be considerably larger on the ferromagnetic $(J_1 < 0)$ side of the CAF sector. This will be further discussed in Sec. V.

D. First-order quantum corrections to the magnetic susceptibility

In the spin-wave approximation, the magnetization curve for the simple AF exhibits a logarithmic singularity of the slope close to the saturation field h_s as shown in Refs. 13 and 23. This should be more easily visible in the high field susceptibility. Furthermore, for ϕ approaching a classical phase boundary, the low field susceptibility has to vanish, which signifies the instability of the order parameter. For these reasons, we found it useful to study the magnetic susceptibility $\chi(h,\phi) = \partial m(h,\phi)/\partial h$ as a function of the frustration angle ϕ in addition to the magnetization. From Eq. (13), we obtain

$$\chi(h,\phi) = \chi_0 + \chi_{zp} = \frac{S}{h_s} - \frac{1}{2N}\sum_k \left(\frac{\partial^2 \epsilon_{\mathbf{k}}(h)}{\partial h^2}\right). \tag{18}$$

From Eq. (12) and using $(\partial A_{\mathbf{k}}/\partial h) = 0$, we arrive at

$$\frac{\partial^2 \epsilon_{\mathbf{k}}(h)}{\partial h^2} = \left(\frac{\partial \epsilon_{\mathbf{k}}}{\partial h}\right)\left[\frac{1}{h} - \frac{1}{\epsilon_{\mathbf{k}}(h)}\left(\frac{\partial \epsilon_{\mathbf{k}}(h)}{\partial h}\right)\right]. \tag{19}$$

Inserting this in Eq. (18) and using Eq. (14) leads to a general expression of the normalized susceptibility $\chi_n(h) = h_s \chi(h)$ according to

$$\chi_n(h,\phi) = S\left[1 - \frac{1}{S}(\Delta\chi_n^{(a)}(h,\phi) - \Delta\chi_n^{(b)}(h,\phi))\right], \tag{20}$$

where the terms $\sim 1/S$ in brackets are the quantum corrections of χ_n^{zp} to the constant classical value $\chi_n^0 = S$. We obtain from Eqs. (18) and (19):

$$\Delta\chi_n^{(a)}(h,\phi) = \frac{S}{h_s}\frac{1}{N}\sum_{\mathbf{k}} c_{\mathbf{k}}\left(\frac{a_{\mathbf{k}} + c_{\mathbf{k}}}{a_{\mathbf{k}} + c_{\mathbf{k}}\cos\theta_c}\right)^{1/2},$$

$$\Delta\chi_n^{(b)}(h,\phi) = 2\frac{S}{h_s}\left(\frac{h}{h_s}\right)^2\frac{1}{N}\sum_{\mathbf{k}} c_{\mathbf{k}}^2\frac{(a_{\mathbf{k}} + c_{\mathbf{k}})^{1/2}}{(a_{\mathbf{k}} + c_{\mathbf{k}}\cos\theta_c)^{3/2}}. \tag{21}$$

For the NAF case, this may be explicitly evaluated as

$$\Delta\chi_n^{(a)}(h,\phi) = \frac{1}{2N}\sum_{\mathbf{k}} \gamma_{\mathbf{k}}\left(\frac{1 + \gamma_{\mathbf{k}} - j(1 - \bar{\gamma}_{\mathbf{k}})}{1 + \gamma_{\mathbf{k}}\cos\theta_c - j(1 - \bar{\gamma}_{\mathbf{k}})}\right)^{1/2},$$

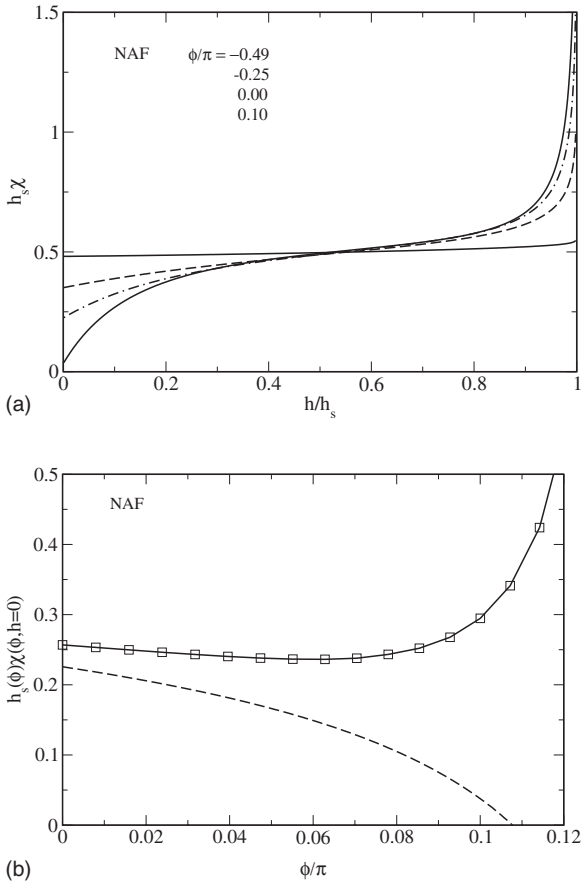

FIG. 3. (a) Susceptibility as a function of field for various ϕ/π values in the NAF sector (ϕ values correspond to curve sequence for $h=0$.) Note the divergence close to h_s for ϕ approaching the sector of the stacked dimer phase. In this regime, the zero-field susceptibility tends to zero, indicating the breakdown of the $(1/S)$ approximation. (b) Zero-field normalized susceptibility χ_n in the $\phi>0$ part of the NAF sector. At $\phi=0$ [see also (a)], the first-order χ_n (dashed line) obtained from Eqs. (20) and (22) is already reduced to half the classical value (equal to S). It decreases further with increasing ϕ and then becomes negative, indicating the instability of the NAF state. Inclusion of second-order contributions in $(1/S)$ stabilizes the positive value (full line, symbols), but they diverge on approaching the CAF/NAF boundary around $\phi/\pi \simeq 0.15$.

$$\Delta\chi_n^{(b)}(h,\phi) = \left(\frac{h}{h_s}\right)^2 \frac{1}{N}\sum_{\mathbf{k}} \gamma_{\mathbf{k}}^2 \frac{(1+\gamma_{\mathbf{k}} - j(1-\bar{\gamma}_{\mathbf{k}}))^{1/2}}{(1+\gamma_{\mathbf{k}}\cos\,\theta_c - j(1-\bar{\gamma}_{\mathbf{k}}))^{3/2}}. \tag{22}$$

Obviously, only the first part $\Delta\chi_n^{(a)}$ contributes to the $(1/S)$ corrections of the zero-field susceptibility. It may also be directly obtained by differentiation of $m(h)$ in Eq. (16). For the CAF case, similar expressions for $\Delta\chi_n^{(a,b)}(h,\phi)$ may be derived by making analogous substitutions in the integrals and their prefactors as done in Eqs. (16) and (17).

The typical field dependence of the susceptibility is shown in Fig. 3. For $\phi/\pi=-0.49$ close to the NAF/FM boundary, one nearly obtains the classical constant value $\chi_n=S$ because, in the FM sector, quantum fluctuations are not present, they are gradually turned on when J_1 becomes positive, and ϕ moves into the NAF sector. This can be clearly seen from the various curves in Fig. 3 (left). For an angle $\phi/\pi=0.1$, frustration becomes large and quantum fluctuations are close to destroying the NAF order. Accordingly, the zero-field susceptibility is close to becoming negative where the spin-wave theory breaks down. One also notes the upturn in the susceptibility just below the critical field coming from the logarithmic singularity of the magnetization.[13,23] The singularity becomes more pronounced when the strongly frustrated point $j=1/2$ is approached.[24]

E. Quantum corrections of the moment canting angle

The angle θ_c between canted AF ordered moments has so far been given in the classical approximation by minimizing only $E_0(\theta_c,h)$. Its quantum corrections of first order in $(1/S)$ may be computed by minimizing the total energy $E_0(\theta_c,h)+E_{zp}(\theta_c,h)$, keeping θ_c also as a variable in the zero point energy. For the unfrustrated Néel AF, this correction is small; however, as we shall see in the following, it may be of considerable size close to the classical boundaries of NAF and CAF phases where frustration effects are large.

The equilibrium condition including quantum corrections is given by

$$\frac{\partial E_0}{\partial\theta_c} + \frac{1}{2N}\sum_{\mathbf{k}}\left(\frac{\partial\epsilon_{\mathbf{k}}}{\partial\theta_c} - \frac{\partial A_{\mathbf{k}}}{\partial\theta_c}\right) = 0. \tag{23}$$

Now θ_c is to be treated as a variable present in $\epsilon_{\mathbf{k}}$ and $A_{\mathbf{k}}$. The form of $A_{\mathbf{k}}$ in Eqs. (9) and (10) already has the classical angle of Eq. (7) substituted. Its general form is $A_{\mathbf{k}}=Sa_{\mathbf{k}}$, with

$$a_{\mathbf{k}} = -4J_2(1-\bar{\gamma}_{\mathbf{k}}) - 4J_1\cos\,\theta_c + h\cos\frac{\theta_c}{2} \tag{24}$$

for the NAF case. Likewise, for the CAF sector, one obtains

$$a_{\mathbf{k}} = -2J_1(1-\gamma_y) - 2(J_1+2J_2)\cos\,\theta_c + h\cos\frac{\theta_c}{2}. \tag{25}$$

Evaluating the derivatives of $\epsilon_{\mathbf{k}}$ and $A_{\mathbf{k}}$ with respect to θ_c and solving the equilibrium Eq. (23), we obtain the canting angle θ_c' renormalized by quantum fluctuations:

$$\cos\frac{\theta_c'}{2} = \cos\frac{\theta_c}{2}\left\{1 - \frac{1}{h_s}\frac{1}{N} \times\sum_{\mathbf{k}}\left[\frac{a_{\mathbf{k}}^{(1)}\left(a_{\mathbf{k}}+c_{\mathbf{k}}\cos^2\frac{\theta_c}{2}\right)+c_{\mathbf{k}}(a_{\mathbf{k}}+c_{\mathbf{k}})}{(a_{\mathbf{k}}+c_{\mathbf{k}})^{1/2}(a_{\mathbf{k}}+c_{\mathbf{k}}\cos\,\theta_c)^{1/2}} - a_{\mathbf{k}}^{(1)}\right]\right\}. \tag{26}$$

Here, $\cos\frac{\theta_c}{2}=h/h_s$ is the classical canting angle and $a_{\mathbf{k}}^{(1)}=-(h_s/2S)$ is the coefficient of the second term in Eqs. (24) and (25). Again, because of $h_s=2S(a_\parallel+a_\perp)$, the term $\sim 1/h_s$ in Eq. (26) has to be considered as a $(1/S)$ correction to the canting angle. Therefore, in the sum on the right-hand side, the classical values for θ_c have to be used, which again lead to the intrasublattice coupling $a_{\mathbf{k}}$ as given by Eq. (10).

The general solution in Eq. (26) is valid for both AF phases. In the NAF case, it leads to the explicit result

$$\cos\frac{\theta_c'}{2} = \cos\frac{\theta_c}{2}\left\{1 - \frac{1}{2SN}\sum_{\mathbf{k}}\left[\frac{\gamma_{\mathbf{k}}^2 + \gamma_{\mathbf{k}}\sin^2\frac{\theta_c}{2} - 1 + j(1-\bar{\gamma}_{\mathbf{k}})(1-\gamma_{\mathbf{k}})}{(1+\gamma_{\mathbf{k}} - j(1-\bar{\gamma}_{\mathbf{k}}))^{1/2}(1+\gamma_{\mathbf{k}}\cos\theta_c - j(1-\bar{\gamma}_{\mathbf{k}}))^{1/2}} + 1\right]\right\}. \quad (27)$$

For the simple AF ($j=0$), one recovers the expression given in Ref. 13. A similar explicit expression for the CAF case may be derived, but it is too unwieldy to be given here. For the numerical calculation of $\cos\frac{\theta_c'}{2}$, Eq. (26) may be used as well.

The field dependence of renormalized moment canting given by $\cos\frac{\theta_c'}{2}$ in comparison with the normalized magnetization $m(h)/S$ is shown in Fig. 4. Generally, the quantum corrections to the canting angle are quite small deep inside the AF sectors. As for the magnetization, they become larger when approaching a phase boundary. Interestingly, however, they may have different signs for the former (left panel), while they must always be negative for the latter (right panel). The positive correction to $\cos\frac{\theta_c'}{2}$ appears in the vicinity of the NAF/CAF boundary.

The quantum corrections to magnetization and canting angle may be used to obtain the correction to the moment size. Classically, we have $S=m_0/\cos\frac{\theta_c}{2}$. If we use a similar definition including the quantum corrections, we have $\langle S\rangle = m/\cos\frac{\theta_c'}{2}$ for the renormalized moment. The change of moment size defined by $\delta S = S - \langle S\rangle$ is then given by $\delta S = S - (m/\cos\frac{\theta_c'}{2})$. Note, however, that in this relation the quantum correction to S formally contains effects of arbitrary order in $(1/S)$ even if m and $\cos\frac{\theta_c'}{2}$ are only corrected in order $(1/S)$. Close to the nonmagnetic regions, when m approaches zero, $\delta S/S$ becomes unity, i.e., the staggered moment is destroyed by the quantum fluctuations.

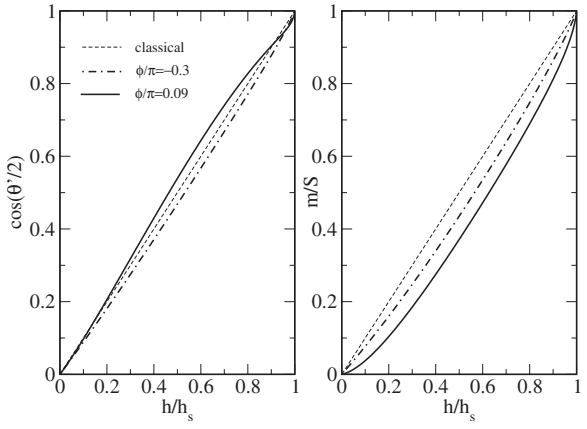

FIG. 4. Comparison of $(1/S)$ quantum corrected canting angle θ_c' (left) and magnetization (right) for two values in the NAF sector. It is seen that first-order quantum corrections always reduce the magnetization with respect to the classical value according to Eq. (15). For $\cos(\theta_c'/2)$, however, the corrections may have both signs. They are small and negative for ϕ deep in the NAF sector, while they are positive closer to the NAF/CAF boundary.

F. Second-order spin-wave results for the magnetization and susceptibility

The linear spin wave theory used in the previous sections includes the leading contribution to the ground-state energy $\sim\mathcal{O}(S)$ [see Eq. (3)]. The next order contributions to $E_{\text{g.s.}}$ come from (i) the canting angle renormalization, (ii) a Hartree–Fock decoupling of the quartic terms, and (iii) the cubic terms. The detailed derivation in the case of nonfrustrated square-lattice AF is given in Ref. 13. Here, we present only the final result for the Néel phase of the J_1-J_2 model. The ground-state energy per site in second-order spin-wave theory consists of the classical part E_0, first-order corrections (zero point fluctuations) E_{zp}, and second order in $1/S$ corrections. In total, it may be written as

$$\begin{aligned} E_{\text{g.s.}}/N = &-2(J_1 - J_2)S(S+1) - \frac{h^2}{16J_1} + \frac{1}{2N}\sum_{\mathbf{k}}\epsilon_{\mathbf{k}} \\ &- 2J_1[(n-\delta_1)^2 + n_1(n_1-\delta)] \\ &+ 2J_2[(n-n_2)^2 + \delta_2(\delta_2-\delta)] \\ &+ 4J_1\cos^2(\theta_c/2)\left[\left(n - \frac{1}{2}\delta\right)(\delta_1+n_1) - 2\delta_1 n_1\right] \\ &- J_1\sin^2\theta_c\frac{1}{3N^2}\sum_{\mathbf{k},\mathbf{q}}\frac{F(\mathbf{k},\mathbf{q})^2}{\epsilon_{\mathbf{k}}+\epsilon_{\mathbf{q}}+\epsilon_{\mathbf{k}+\mathbf{q}-\mathbf{Q}}}. \end{aligned} \quad (28)$$

Here, the first line is equal to the sum of E_0+E_{zp}, while the rest constitutes the second order in $1/S$ spin-wave contribution. In this term, the six constants are given by two-dimensional momentum integrals as follows:

$$n = \frac{1}{N}\sum_{\mathbf{k}}\frac{A_{\mathbf{k}} + C_{\mathbf{k}} - \epsilon_{\mathbf{k}}}{2\epsilon_{\mathbf{k}}},$$

$$n_{1(2)} = \frac{1}{N}\sum_{\mathbf{k}}\gamma_{\mathbf{k}}(\bar{\gamma}_{\mathbf{k}})\frac{A_{\mathbf{k}} + C_{\mathbf{k}}}{2\epsilon_{\mathbf{k}}},$$

$$\delta = \frac{1}{N}\sum_{\mathbf{k}}\frac{B_{\mathbf{k}}}{2\epsilon_{\mathbf{k}}}, \quad \delta_{1(2)} = \frac{1}{N}\sum_{\mathbf{k}}\gamma_{\mathbf{k}}(\bar{\gamma}_{\mathbf{k}})\frac{B_{\mathbf{k}}}{2\epsilon_{\mathbf{k}}}, \quad (29)$$

while the expression for the cubic vertex $F(\mathbf{k},\mathbf{q})$ is given by Eq. (25) in Ref. 13. The magnetization curve is obtained by the numerical differentiation $m=-\partial E_{\text{g.s.}}(h)/\partial h$.

The effect of the second-order contributions in the magnetization may be seen in Fig. 5 and also in Fig. 2 in the comparison to the ED Lanczos results. In general, the second-order spin-wave corrections to the first order in $(1/S)$ results are positive for small fields and negative for large fields (Fig. 5). As long as ϕ is within the stable antiferromagnetic sectors, the second-order corrections are quite small. For example, when $\phi/\pi=-0.21,-0.17,0.41$, the first-

and second-order results are almost indistinguishable to the eye and agree with Lanczos results (Fig. 2). When ϕ approaches the strongly frustrated phase boundaries, the first-order approximation breaks down as witnessed by the magnetization becoming negative (Figs. 2 and 5). The second-order corrections remedy this situation. However, close to the boundaries, they become very large, leading to a very anomalous low field second-order magnetization which deviates strongly from the Lanczos results (Fig. 2). Since the deviations between the first- and second-order curves are strongly enhanced close to the classical phase boundaries, it is clear that spin-wave expansion no longer converges. In Fig. 2, this is obvious for $\phi/\pi=0.17$ at the NAF/CAF boundary and even more so for $\phi/\pi=0.75$, already well in advance of the CAF/FM boundary at $\phi/\pi=0.85$. In fact, the first-order result (full line) agrees better with the Lanczos results (full symbols) plotted for comparison than does the second-order curve (dotted line).

Finally, from Eq. (29) the second order in $(1/S)$ corrections to the zero-field susceptibility may be calculated in addition to the first-order expression given in Eqs. (20) and (22). The comparison of first- and second-order results for the NAF case is given in Fig. 3 (right panel). Although the second-order contributions repair the negative instability of the first-order susceptibility at $\phi \simeq 0.11\pi$, the second-order result itself diverges when one moves even closer to the classical phase boundary at $\phi \simeq 0.15\pi$.

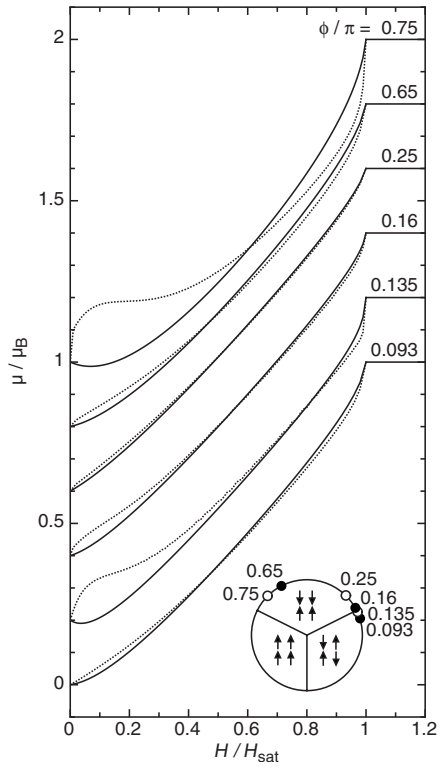

FIG. 5. Compiled comparison of first (full lines) and second (dotted lines) order in $(1/S)$ spin-wave results for the magnetization for various frustration angles indicated in the inset. An offset of 0.2 has been applied. Curves in increasing order correspond to ϕ values in the counterclockwise direction. Well inside the antiferromagnetic regimes ($\phi/\pi=0.093, 0.25, 0.65$), the first- and second-order results show little difference. Close to the classical phase boundaries ($\phi/\pi=0.135, 0.16, 0.75$), the first-order results lead to unstable (negative) low field magnetization. The instability region below $\phi/\pi=0.85$ (CAF/FM) is much larger than around $\phi/\pi=0.15$ (NAF/CAF). The second-order results are always positive, but show very anomalous low field magnetization contrary to the Lanczos results in Fig. 2. Note that the second-order corrections in $(1/S)$ to the first-order curves are positive for low fields and negative for large fields.

IV. EFFECT OF INTERLAYER EXCHANGE COUPLING

In real magnetic systems, other interactions may play a certain role besides the in-plane Heisenberg exchange. These include various anisotropies as well as a three-dimensional coupling. We shall consider modifications of the above formulas produced by interlayer exchange coupling as

$$\mathcal{H}_\perp = J_\perp \sum_{\langle ij\rangle_z} \mathbf{S}_i \cdot \mathbf{S}_j \tag{30}$$

for nearest-neighbor spins in the direction perpendicular to the layers. (Note the different convention for field direction in Sec. III B). Here, we assume the simple stacking of the layers. The obtained results can be easily extended to other cases as well.

For ferromagnetic exchange $J_\perp<0$, the saturation field for NAF is still given by $h_s=8SJ_1$, while for antiferromagnetic exchange $J_\perp>0$, it is given by $h_s=8SJ_1(1+\frac{1}{2}j_\perp)$. Here, we define $j_\perp=J_\perp/J_1$. The first-order spin-wave result for the magnetization in the NAF case which includes the interplanar coupling $J_\perp$ is given by

$$J_\perp<0: \quad m = S\frac{h}{h_s}\left[1-\frac{1}{2SN}\sum_{\mathbf{k}}\gamma_{\mathbf{k}}\left(\frac{1+\gamma_{\mathbf{k}}-j(1-\bar{\gamma}_{\mathbf{k}})+\frac{1}{2}|j_\perp|(1-\gamma_z)}{1+\gamma_{\mathbf{k}}\cos\theta_c-j(1-\bar{\gamma}_{\mathbf{k}})+\frac{1}{2}|j_\perp|(1-\gamma_z)}\right)^{1/2}\right],$$

$$J_\perp>0: \quad m = S\frac{h}{h_s}\left[1-\frac{1}{2SN}\sum_{\mathbf{k}}\frac{\eta_{\mathbf{k}}}{1+\frac{1}{2}j_\perp}\left(\frac{1+\frac{1}{2}j_\perp+\eta_{\mathbf{k}}-j(1-\bar{\gamma}_{\mathbf{k}})}{1+\frac{1}{2}j_\perp+\eta_{\mathbf{k}}\cos\theta_c-j(1-\bar{\gamma}_{\mathbf{k}})}\right)^{1/2}\right]. \tag{31}$$

Here, $\eta_{\mathbf{k}}=\gamma_{\mathbf{k}}+\frac{1}{2}j_\perp\cos k_z$ is the three-dimensional (3D) structure factor and summation is now extended over a 3D Brillouin zone.

In the case of CAF order, the first-order spin-wave theory for a ferromagnetic interlayer exchange $J_\perp<0$ leads to $h_s=4SJ_1(1+2j)$, and for an antiferromagnetic case $J_\perp>0$, the saturation field is given by $h_s=4SJ_1(1+2j+4j_\perp)$. The first-order spin-wave result for the magnetization in the 3D CAF case is then obtained as

$$J_\perp<0: \quad m=S\frac{h}{h_s}\left[1-\frac{1}{2SN}\sum_{\mathbf{k}}\frac{j\bar{\gamma}_{\mathbf{k}}+\frac{1}{2}\gamma_x}{j+\frac{1}{2}}\left(\frac{j(1+\bar{\gamma}_{\mathbf{k}})+\gamma_{\mathbf{k}}+\frac{1}{2}|j_\perp|(1-\gamma_z)}{j(1+\bar{\gamma}_{\mathbf{k}}\cos\theta_c)+\frac{1}{2}(\gamma_y+\cos\theta_c\gamma_x)+\frac{1}{2}|j_\perp|(1-\gamma_z)}\right)^{1/2}\right],$$

$$J_\perp<0: \quad m=S\frac{h}{h_s}\left[1-\frac{1}{2SN}\sum_{\mathbf{k}}\frac{j\bar{\gamma}_{\mathbf{k}}+\frac{1}{2}\gamma_x+\frac{1}{2}j_\perp\gamma_z}{j+\frac{1}{2}(1+j_\perp)}\left(\frac{j(1+\bar{\gamma}_{\mathbf{k}})+\gamma_{\mathbf{k}}+\frac{1}{2}j_\perp(1+\gamma_z)}{j(1+\bar{\gamma}_{\mathbf{k}}\cos\theta_c)+\frac{1}{2}(\gamma_y+\cos\theta_c\gamma_x)+\frac{1}{2}j_\perp(1+\gamma_z\cos\theta_c)}\right)^{1/2}\right]. \quad (32)$$

Here, we used the convention $\gamma_i=\cos k_i$ $(i=x,y,z)$.

We have verified that for well-ordered NAF and CAF phases, the effect of interlayer coupling is hardly visible up to $|J_\perp|\sim 0.3|J_{1,2}|$. This means that the application of our first-order spin-wave results to real compounds does not critically depend on a small interlayer coupling $J_\perp$ as long as the quantum antiferromagnet is in a well-ordered phase. Closer to the phase boundaries, $J_\perp$ has the effect of stabilizing the ordered phases, especially for $J_\perp<0$.

V. DISCUSSION AND CONCLUSION

In this work, we have explored the quantum corrections to the magnetization, the uniform susceptibility, and the canting angle in the first- and second-order spin-wave approximations and by using an exact diagonalization of finite clusters. The deviations from classical behavior were found to be pronounced close to the strongly frustrated regions where the classical phases meet. Indeed, we have shown that linear spin-wave theory breaks down in these regions and the second-order corrections do not fundamentally change this observation. The latter are small well within the AF regions and have a positive sign for small fields and a negative sign for large fields. Although they prevent the instability of the linear spin-wave theory for small fields, they become very anomalous close to the boundaries and one cannot expect that the $1/S$ expansion converges in the nonmagnetic region. This is intuitively clear since the spin-wave expansion in the region of the classical boundaries starts from the wrong, i.e., magnetically ordered, ground state.

A striking feature of these results is that the deviations from classical behavior in the magnetization curve $m(h)$ and the breakdown of the spin-wave expansion are most pronounced on the ferromagnetic side $(J_1<0)$, as illustrated in Figs. 2 and 5. One can understand this by considering the asymptotic form of the first-order corrections to the staggered moments δS and the uniform susceptibility $\delta\chi$ in the CAF phase as $j\to\pm 1/2$:

$$\delta S\simeq\sum_{\mathbf{k}}\frac{1}{\sqrt{k_x^2+|\delta j|k_y^2}},$$

$$\delta\chi\simeq\frac{1}{j+\frac{1}{2}}\sum_{\mathbf{k}}\frac{1}{\sqrt{k_x^2+|\delta j|k_y^2}}. \quad (33)$$

Here, $\delta j=j\pm\frac{1}{2}$ is the deviation from one of the two strongly frustrated points. For the CAF/NAF boundary, the diverging corrections are the same for the sublattice magnetization and the susceptibility $\delta S,\delta\chi\sim\ln|\delta j|$. For the CAF/FM frustration point, the susceptibility correction acquires an additional diverging prefactor $\delta\chi\sim(\ln|\delta j|)/(\delta j)$, which indicates that a long-range magnetic order is destabilized in a much wider window of J_2/J_1 for this sign of J_1.

This is in accordance with the ED Lanczos results where a tendency to bound state formation of spin waves, as indicated by the $\Delta S_z=2$ steps in the magnetization of finite clusters, is observed.[11] This is evidence that around $\phi\simeq 0.85\pi$ or $J_2/J_1\simeq -0.5$ the ground state will be of the spin-nematic type as proposed in Ref. 12. It may be viewed as a quantum gapless phase, with a Goldstone mode describing the collective long-range excitations of a nonlocal quadrupolar order parameter. A second-order transition between the CAF phase and this spin nematic *is* permitted by the symmetry of the order parameter, and the smooth evolution of ED spectra across the transition suggests that a second order does, in fact, occur. The pronounced quantum fluctuations seen in spin-wave theory lend further support to this idea.

This can be most clearly seen in Fig. 6 (left panel), where the magnetization is plotted as a function of the frustration angle ϕ. The decrease in magnetization from the classical value $m/S=h/h_s$ at around half-saturation $(h/h_s=0.58)$ characterizes the strength of quantum fluctuations. Their effect increases from zero at FM/NAF boundary to a maximum at NAF/CAF boundary, where a discontinuous jump in the magnetization occurs. For $\phi/\pi>0.5$ (the CAF regime with $J_2<0$), the reduction of m/S due to quantum fluctuations rapidly becomes large and the expansion in $1/S$ breaks down. This is also seen in Fig. 5.

The exact numerical results (circles) obtained from the Bonner–Fisher plots (hence, the steps) as in Fig. 1 also show the strong reduction of the magnetization close to the classical CAF/FM boundary. This is a signature of the true spin-nematic quantum ground state which does not break time reversal symmetry. Therefore, it has no first-order (linear) coupling to the magnetic field, resulting in a small magnetization. The right panel of Fig. 6 shows the comparison of high field susceptibility at $h=h_s^-(\phi)$ from first-order spin-wave theory (full line) at $T=0$ with the ED Lanczos results at small but finite T, plotted as a function of the frustration angle ϕ. The susceptibility in both cases is normalized to the pure NAF case $(\phi=0)$. The overall agreement of ϕ dependence is quite good because, due to high fields, the effect of

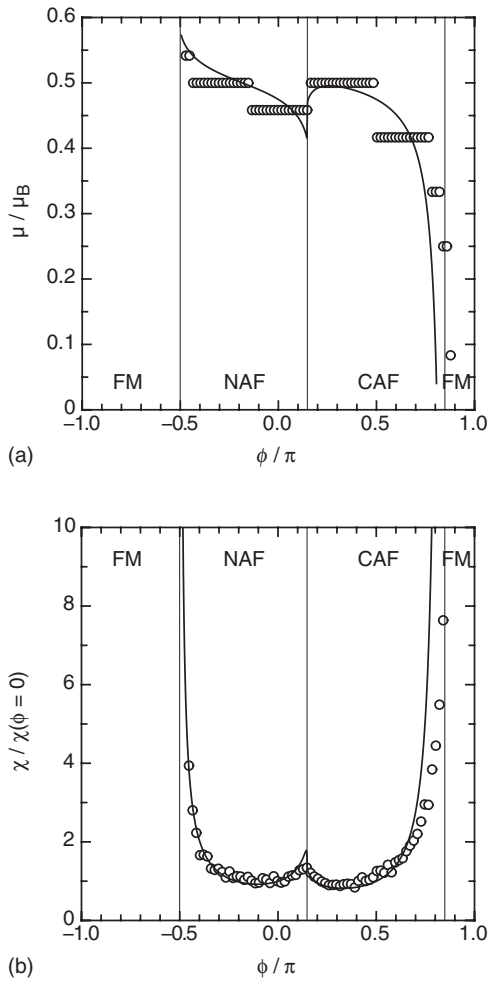

FIG. 6. (a) Variation of the moment $\mu/\mu_B=gm$ as a function of ϕ for $h/h_s=0.58$ close to half-saturation. Circles are obtained from the Bonner–Fisher plots based on numerical ($T=0$) Lanczos results. Full lines include the $(1/S)$ quantum correction from spin-wave excitations according to Eq. (15) with respect to the constant classical value $\mu/\mu_B=m/S=0.58$. At the FM/NAF boundary where the quantum fluctuations are small, the magnetization starts at this value and then is continuously reduced as one approaches the strongly frustrated sector around the NAF/CAF boundary. There the magnetization jumps to a slightly larger value and then breaks down close to the spin-nematic region around the CAF/FM boundary. (b) Susceptibility $\chi(\phi)/\chi(\phi=0)$ for $h=h_s^-(\phi)$ normalized to the simple NAF value. Circles are ED Lanczos results ($k_BT/J_c=0.2$) and full lines are $T=0$ spin-wave results according to Eq. (20).

quantum fluctuations is suppressed. Again, the deviations are strongest close to the classical CAF/FM boundary, where the saturation field approaches zero and the spin-wave approximation breaks down.

The deviations from classical results and the breakdown of the spin-wave approximation are much less severe on the CAF/NAF phase boundary at the AF side ($J_1>0$). The magnetization behaves significantly less singular in this region. As mentioned before, a discontinuous jump in $m(\phi)$ at $\phi \simeq 0.15\pi$ occurs at around half-saturation (Fig. 6). Then the quantum phase transition to the presumably stacked spin dimer ground state may be expected to be a first-order transition. Therefore, the magnetic and nonmagnetic phases on both sides of the boundary will correspond to stable local minima of the free energy and fluctuations will not be very pronounced, leading to a less singular magnetization behavior. The first-order nature of transition between CAF and a nonmagnetic columnar-dimer state was noticed in an earlier numerical work,[16] while for the boundary with the NAF, a first-order scenario was only recently put forward.[18]

Finally, we comment on experimental data for the high field magnetization of J_1-J_2 compounds. There are no published data for those systems mentioned in the Introduction. However, recently, a new compound $(CuBr)LaNb_2O_7$, with a perovskite/metal halide intergrowth structure, was synthesized.[25] This is a spin-1/2 magnetic insulator, and is reported to exhibit quasi-2D magnetic behavior arising from the CuBr–square-lattice planes. It shows CAF order at a relatively large $T_N=32$ K.

It has been suggested that the magnetism of $(CuBr)LaNb_2O_7$ can be described by the square-lattice J_1-J_2 model with a frustration angle $\phi=0.73\pi$ $(J_2/J_1=-1.1)$, which puts this compound closer to the strongly frustrated region of the spin-nematic phase than any other compound reported so far. Our spin-wave calculations predict a pronounced nonlinear magnetization for this parameter set, particularly at low fields. However, the experimental results in Ref. 25 show only a modest curvature at high fields. We, therefore, conclude that, while these materials likely do possess competing FM and AF interactions, they probably cannot be described by a simple square-lattice J_1-J_2 model.

Various further extensions of the model (besides interlayer coupling) are possible: inclusion of in-plane exchange anisotropy to describe orthorhombic distortions, asymmetric exchange, and four-spin ring exchange. Each extension requires a separate analysis of possible ordered states and their corresponding spin-wave excitations.

In conclusion, it is abundantly clear that classically disordered phases of the square-lattice J_1-J_2 model need and deserve an analysis which goes beyond the spin-wave theory presented here. This is further motivated by the fact that some of the known J_1-J_2 vanadium compounds are rather close to the spin-nematic sector of the phase diagram. For further progress to be made in understanding the hidden order phases, an approximative treatment of the broken order parameter and its low lying excitations is necessary. Since both the dimer and nematic phases are bond centered, the bond-operator method might be a useful choice.

ACKNOWLEDGMENTS

We are pleased to acknowledge helpful conversations with C. Geibel, Tsutomu Momoi, and Luis Seabra. This work was supported in part by the SFB 463 project of DFG (P.T., N.S.) and by EPSRC-GB (Grant No. EP/C539974/1) (N.S.). M.E.Z. is grateful to Max Planck Institute PKS for hospitality in the course of this work.

[1] G. Misguich and C. Lhuillier, in *Frustrated Spin Systems*, edited by H. T. Diep (World Scientific, Singapore, 2004).
[2] A. Läuchli, J. C. Domenge, C. Lhuillier, P. Sindzingre, and M. Troyer, Phys. Rev. Lett. **95**, 137206 (2005).
[3] G. Misguich and P. Sindzingre, Eur. Phys. J. B **59**, 305 (2007).
[4] P. Millet and C. Satto, Mater. Res. Bull. **33**, 1339 (1998).
[5] R. Melzi, P. Carretta, A. Lascialfari, M. Mambrini, M. Troyer, P. Millet, and F. Mila, Phys. Rev. Lett. **85**, 1318 (2000).
[6] R. Melzi, S. Aldrovandi, F. Tedoldi, P. Carretta, P. Millet, and F. Mila, Phys. Rev. B **64**, 024409 (2001).
[7] E. E. Kaul, H. Rosner, N. Shannon, R. V. Shpanchenko, and C. Geibel, J. Magn. Magn. Mater. **272-276**, 922 (2004).
[8] E. Kaul, Ph.D. thesis, Technische Universität Dresden, 2005.
[9] N. Kini, E. E. Kaul, and C. Geibel, J. Phys.: Condens. Matter **18**, 1303 (2006).
[10] N. Shannon, B. Schmidt, K. Penc, and P. Thalmeier, Eur. Phys. J. B **38**, 599 (2004).
[11] B. Schmidt, P. Thalmeier, and N. Shannon, Phys. Rev. B **76**, 125113 (2007).
[12] N. Shannon, T. Momoi, and P. Sindzingre, Phys. Rev. Lett. **96**, 027213 (2006).
[13] M. E. Zhitomirsky and T. Nikuni, Phys. Rev. B **57**, 5013 (1998).
[14] M. P. Gelfand, R. R. P. Singh, and D. A. Huse, Phys. Rev. B **40**, 10801 (1989).
[15] S. Sachdev and R. N. Bhatt, Phys. Rev. B **41**, 9323 (1990).
[16] H. J. Schulz and T. A. L. Ziman, Europhys. Lett. **18**, 355 (1992).
[17] V. N. Kotov, J. Oitmaa, O. P. Sushkov, and Zheng Weihong, Phys. Rev. B **60**, 14613 (1999).
[18] J. Sirker, Z. Weihong, O. P. Sushkov, and J. Oitmaa, Phys. Rev. B **73**, 184420 (2006).
[19] M. S. Yang and K. Mütter, Z. Phys. B: Condens. Matter **104**, 117 (1997).
[20] J. C. Bonner and M. S. Fisher, Phys. Rev. **135**, A640 (1964).
[21] M. E. Zhitomirsky, A. Honecker, and O. A. Petrenko, Phys. Rev. Lett. **85**, 3269 (2000).
[22] A. Honecker, Can. J. Phys. **79**, 1557 (2001).
[23] S. Gluzman, Z. Phys. B: Condens. Matter **90**, 313 (1993).
[24] G. Jackeli and M. E. Zhitomirsky, Phys. Rev. Lett. **93**, 017201 (2004).
[25] N. Oba, H. Kageyama, T. Kitano, J. Yasuda, Y. Baba, M. Nishii, K. Hirota, Y. Narumi, M. Hagiwara, K. Kindo, T. Saito, Y. Ajiro, and K. Yoshimura, J. Phys. Soc. Jpn. **75**, 113601 (2006).